Preclinical investigation of potential use of thymidine phosphorylase imaging probe for diagnosis of nonalcoholic steatohepatitis

Kei Higashikawa[1,2,*], Sawako Horiguchi[3], Makoto Tarisawa[3], Yuki Shibata[2], Kazue Ohkura[4], Hironobu Yasui[1,2], Hiroshi Takeda[3], Yuji Kuge[1,2]

[1]Central Institute of Isotope Science, Hokkaido University, Hokkaido 060-0815, Japan

[2]Graduate School of Biomedical Science and Engineering, Hokkaido University, Hokkaido 060-0815, Japan

[3]Faculty of Pharmaceutical Sciences, Hokkaido University, Hokkaido 060-0812, Japan

[4]Faculty of Pharmaceutical Sciences, Health Sciences University of Hokkaido, Hokkaido 061-0293, Japan

Running title: Decreased hepatic accumulation levels of TYMP imaging probe

***Corresponding Author:**

Kei Higashikawa, Ph.D.

Central Institute of Isotope Science, Hokkaido University

Kita 15, Nishi 7, Kita-ku, Sapporo, Hokkaido 060-0815, Japan

19 Tel.: +81-11-706-6092

20 Fax: +81-11-706-7862

21 E-mail: higahikawa@ric.hokudai.ac.jp

22

23

Abstract

[Introduction]

Although liver biopsy is the gold standard for the diagnosis of nonalcoholic steatohepatitis (NASH), it has several problems including high invasiveness and sampling errors. Therefore, the development of alternative methods to overcome these disadvantages is strongly required. In this study, we evaluated the potential use of our imaging probe targeting thymidine phosphorylase (TYMP), [^{123}I]5-iodo-6-[(2-iminoimidazolidinyl)methyl]uracil ([^{123}I]IIMU) for the diagnosis of NASH.

[Methods]

The mice used as the NASH model (hereafter, NASH mice) were prepared by feeding a methionine- and choline-deficient diet for 4 weeks. A control group was similarly given a control diet. The expression levels of the TYMP gene and protein in the liver were examined by real-time reverse-transcription polymerase chain reaction and western blot analyses. The localizations of [^{125}I]IIMU and the TYMP protein in the liver were examined by autoradiography and immunohistochemical staining, respectively.

Finally, the mice were injected with [^{123}I]IIMU and single-photon emission tomography (SPECT) imaging was conducted.

[Results]

The hepatic expression levels of TYMP were significantly lower in the NASH mice than in the control mice at both mRNA and protein levels, suggesting that a decrease in TYMP level could be an indicator of NASH. [^{125}I]IIMU was uniformly distributed in the liver of the control mice, whereas it showed a patchy distribution in that of the NASH mice. The localization of [^{125}I]IIMU was visually consistent with that of the TYMP protein in the liver of the control and NASH mice. SPECT analysis indicated that the hepatic accumulation of [^{123}I]IIMU in the NASH mice was significantly lower than that in the control mice [SUV (g/ml): 4.14 ± 0.87 (Control) vs 2.31 ± 0.29 (NASH)].

[Conclusions]

[^{123}I]IIMU may provide a noninvasive means for imaging TYMP expression in the liver and may be applicable to the diagnosis of NASH.

60 KEYWORDS: NASH, TYMP, IIMU, Imaging

61

1. Introduction

Nonalcoholic fatty liver disease (NAFLD) is one of the most common chronic liver diseases affecting people who drink little to no alcohol. NAFLD covers a spectrum of conditions ranging from simple steatosis, which follows a benign clinical course, to nonalcoholic steatohepatitis (NASH), which progresses to liver fibrosis, cirrhosis, and hepatocellular carcinoma (HCC). Although progress has been made in the development of diagnostic methods for NASH, liver biopsy is the only reliable method to accurately diagnose and stage NAFLD/NASH severity [1]. However, liver biopsy has many drawbacks such as high invasiveness (risk of complications) and interobserver variability [2, 3]. In addition, biopsy sample is so small that diagnostic results tend to be different depending on the biopsy site (sampling errors) [4]. Therefore, it is not realistic to perform liver biopsies on all NAFLD patients, and the development of alternative methods to overcome these disadvantages is urgently desired.

Nuclear medicine imaging technologies with single-photon emission tomography (SPECT) and positron emission tomography (PET) enable the direct and noninvasive evaluation of whole organs. Therefore, diagnosis using these technologies has a

potential to become a reliable method to accurately diagnose and stage NAFLD/NASH severity if appropriate imaging biomarkers are found.

Tumor necrosis factor (TNF)-α plays a pivotal role in the development of fatty liver and subsequently NASH [5]. Treatment with TNF-α antibodies improved fatty liver formation and hepatic inflammation [6]. Therefore, factors induced by TNF-α may have the potential to be imaging biomarkers of NASH. Thymidine phosphorylase (TYMP) is induced by TNF-α and is also identical to the platelet-derived endothelial cell growth factor (PD-ECGF) [7, 8]. We previously synthesized radioiodine-labeled [$^{123/125}$I]5-iodo-6-[(2-iminoimidazolidinyl)methyl]uracil (IIMU), a potent inhibitor of thymidine phosphorylase (TYMP) (Fig. 1) [9]. [$^{123/125}$I]IIMU accumulated in rodent tumor cells and tissues, depending on TYMP expression level [10-13], and was safely administered in humans [14].

From these reports, we hypothesized that TYMP may function as an imaging biomarker of NASH, and [^{123}I]IIMU provides a noninvasive means for imaging NASH. In this study, we aimed to investigate the feasibility of TYMP as an imaging biomarker of NASH, and we also evaluated the potential use of [^{123}I]IIMU for the diagnosis of NASH.

2. Materials and Methods

2-1. Preparation of mouse NASH model

Male C57BL/6N mice were purchased from Japan SLC, Inc. (Hamamatsu, Japan). The mice were housed under a 12-h light/12-h dark cycle with food and water supplied ad libitum. All experimental protocols were approved by the Laboratory Animal Care and Use Committee of Hokkaido University and performed in accordance with the Guidelines for Animal Experiments of the Graduate School of Medicine, Hokkaido University.

The mice (8 weeks old) were housed with control diet (A02082003B, Research Diets Inc., New Brunswick, NJ) for at least 1 week, and then they were divided into two groups, the NASH model and the control. The mice used as the NASH model (hereafter, NASH mice) were prepared by feeding a methionine/choline-deficient (MCD) diet (A02082002B, Research Diet, Inc.) for 4 weeks. The control group was maintained on the original diet for 4 weeks.

2.2. Physiological and biochemical assays

116

117 The NASH and control mice were sacrificed under isoflurane anesthesia. Serum was
118 collected and assayed for the levels of alanine aminotransferase (ALT) and aspartate
119 aminotransferase (AST) using an Alanine Aminotransferase (ALT or SGPT) Activity
120 Colorimetric/Fluorometric Assay Kit (BioVision, Inc., Milpitas, CA) and an Aspartate
121 Aminotransferase (AST or SGOT) Activity Colorimetric Assay Kit (BioVision Inc.),
122 respectively, in accordance with the manufacturer's instruction.

123

124 ***2.3. Real-time reverse-transcription polymerase chain reaction (RT-PCR) analysis***

125

126 RNA was extracted by the same methods as in our previous studies [15, 16]. Hepatic
127 total RNA was isolated from the NASH and control mice with TRIZOL® reagent
128 (Thermo Fisher Scientific Inc., Waltham, MA) and purified with a PureLink™ RNA
129 Mini Kit (Thermo Fisher Scientific Inc.). Total RNA (500 ng) was then reversely
130 transcribed using a ReverTra Ace® qPCR RT Master Mix with a gDNA Remover
131 (TOYOBO Co., Ltd., Osaka, Japan) and a PCR Thermal Cycler Dice (Takara Bio Inc.,
132 Kusatsu, Japan). The messenger RNA (mRNA) expression level of TYMP was
133 determined by real-time RT-PCR analysis using TaqMan™ Universal Master Mix II,

with UNG (Thermo Fisher Scientific Inc), primer-probe sets of TaqMan Gene Expression Assays (Mm00460357_m1; Thermo Fisher Scientific Inc.), and Thermal Cycler Dice Real Time System II (Takara Bio Inc.). The expression levels of TNF-α, interleukin-1β (IL-1β), cluster of differentiation 68 (CD68), collagen type I alpha 1 (COA1A1), collagen type I alpha 2 (COA1A2), α-smooth muscle actin (α-SMA), and TATA-binding protein (TBP) were analyzed by real-time RT-PCR using FastStart Universal SYBR Green Master (Rox) (Roche Diagnostics, Indianapolis, IN), the primer set specific for each molecule, and Thermal Cycler Dice Real Time System II. Primer sequences are listed in Supplementary Table S1. The expression level of each mRNA was normalized with that of TBP.

2.4. Histopathological evaluation

The excised livers were fixed in 10% formalin neutral buffer solution (FUJIFILM Wako Pure Chemical Co., Ltd., Osaka, Japan) and embedded in paraffin before sectioning and staining. Five-micrometer-thick liver sections were prepared, deparaffinized in xylene, rehydrated in an ethanol series, and washed in running water. The liver sections were stained with Mayer's hematoxylin solution (FUJIFILM Wako

Pure Chemical Co., Ltd.) and eosin Y solution (Muto Pure Chemicals Co., Ltd., Tokyo, Japan).

2.5. Western blot analysis

The liver tissues were solubilized in RIPA Lysis and Extraction Buffer (Thermo Fisher Scientific, Inc.) containing a protease inhibitor cocktail (cOmplete™, Roche Co., Ltd., Mannheim, Germany). One, ten, and twenty micrograms of the proteins were separated by sodium dodecyl sulfate polyacrylamide gel electrophoresis (SDS-PAGE) on a 5–20% gel (e-PAGEL, ATTO Co., Ltd., Tokyo, Japan) to evaluate the expression levels of TYMP, TBP, and uridine phosphorylase 1 (UPP1) and UPP2, respectively. Recombinant UPP1 (1 ng; Cloud-Clone Co., Katy, TX) and UPP2 (10 ng; Cloud-Clone Co.) were used as positive controls and also similarly separated by SDS-PAGE. Proteins were transferred onto polyvinylidene fluoride membranes (Bio-Rad Laboratories, Inc. Hercules, CA). The membranes were washed with TBS buffer (25 mM Tris–HCl, 137 mM NaCl, 2.68 mM KCl, pH 7.4), and then blocked with TBST buffer (50 mM Tris–HCl, 138 mM NaCl, 2.70 mM KCl, 0.5 ml/L Tween 20, pH 8.0) plus 5% skim milk. The membranes were incubated with a sheep polyclonal anti-TYMP primary

antibody (1:1000; R&D Systems, Inc., Minneapolis, MN) or a rabbit monoclonal anti-TBP primary antibody (1:1000; Cell Signaling Technology Inc., Beverly, MA), an anti-UPP1 primary antibody (1:400; Lifespan Biosciences Inc., Seattle, WA), and an anti-UPP2 primary antibody (1:3000; Abcam, Inc., Cambridge, UK) in TBST buffer plus 5% skim milk. The membranes were washed with TBST buffer and incubated with a horseradish peroxidase (HRP)-conjugated anti-sheep antibody (1:1000; R&D Systems, Inc.) or anti-rabbit antibody (1:4000; Promega Inc., Madison, WI) in TBST buffer plus 5% skim milk. Proteins were visualized and quantified using the Immobilon™ Western Chemiluminescent HRP Substrate (Millipore Inc. Billerica, MA) or ECL Prime Western Blotting Detection Reagent (GE Healthcare Inc., Chicago, IL), and the luminescent image analyzer LAS-4000 mini (Fuji Photo Film Co., Ltd., Tokyo, Japan). TBP was used as the protein-loading control for immunoblotting.

2.6 Biodistribution study

Approximately 2.6 MBq/kg [^{125}I]IIMU in saline was intravenously administered to the NASH and control mice via the tail vein under isoflurane anesthesia. Then, the mice were returned to their cages and allowed to move freely for 30 min. Subsequently, the

188 mice were sacrificed under isoflurane anesthesia, and their organs and blood were
189 immediately removed. After washing the organs with water, the organs and the blood
190 were weighed. The radioactivity in the organs and blood was counted with a gamma
191 counter (2480 WIZARD 2 Automatic Gamma Counter, PerkinElmer Inc., Waltham,
192 MA). Decay-corrected uptake was expressed as standardized uptake value (SUV) and
193 organ-to-blood ratios. SUV was defined as {[tissue radioactivity concentration
194 (Bq/g)/injected radioactivity (Bq)] × body weight (g)}.
195
196 ***2.7. Autoradiography (ARG) and immunohistochemical (IHC) staining analyses***
197
198 The livers were embedded in Optimal Cutting Temperature (O.C.T.) compound
199 (Sakura Finetek Japan Co., Ltd., Tokyo, Japan) and frozen in isopentane/dry ice. For
200 ARG and IHC staining experiments, 20- and 5- to 10-μm-thick serial frozen tissue
201 sections were prepared, respectively. The tissue sections were mounted on MAS-coated
202 glass slides (Matsunami Glass Ind., Co., Ltd., Kishiwada, Japan) and fixed with
203 M-Fix™ spray fixative (Merck, Darmstadt, Germany). For the autoradiography
204 experiment, the liver tissue sections were exposed to a phosphor imaging plate (Fuji
205 Photo Film Co., Ltd.). After the exposure, the imaging plate was scanned with a FLA

7000 Bio-Imaging Analyzer (Fuji Photo Film Co., Ltd.) and the images obtained were analyzed using Multi Gauge V3.0 (Fuji Photo Film Co., Ltd.). For the immunohistochemical staining, the liver tissue sections were washed in 100 mL of phosphate-buffered saline (-) [PBS (-)] containing a drop of 13-fold diluted Triton-X, and blocked with a blocking solution (protein block, serum-free; Agilent Technologies, Inc., Carpinteria, CA). The tissue sections were incubated with an anti-TYMP antibody (1:100; R&D Systems, Inc.) in 0.1% BSA/PBS (-), washed in the PBS (-) plus Triton-X solution, and subjected to endogenous peroxidase inactivation with 0.3% H_2O_2/methanol. Then, the tissue sections were washed in the PBS (-) plus Triton-X solution, incubated with an HRP-conjugated anti-sheep antibody (1:100; R&D Systems, Inc.) in 0.1% BSA/PBS (-), and washed with PBS (-). Immunocomplexes were visualized with a Peroxidase Stain DAB Kit (Nacalai Tesque Inc., Kyoto, Japan) and counterstained with hematoxylin.

2.8. SPECT and computed tomography (CT) analyses

The NASH (n = 4) and control mice (n = 4) were injected with [^{123}I]IIMU (3.3-4.7 MBq) in saline containing 1% ascorbic acid via tail vein under isoflurane anesthesia. At

30 min after the injection, SPECT was performed for approximately 15 min using an Inveon SPECT/CT scanner (Siemens Healthineers Inc., Munich, Germany). A single pinhole collimator set with a 2.0 mm aperture (1-MHS-2.0) were used. Then, CT was performed for attenuation correction. Hepatic accumulation levels of [^{123}I]IIMU were quantified using Inveon Research Workplace (Siemens Healthineers Inc.). To evaluate specific accumulation of [^{123}I]IIMU in the liver, mice were injected with 25 μg tipiracil hydrochloride (TIP; a specific TYMP inhibitor) (SML1552; Sigma-Aldrich Co. Ltd.), into the NASH (n = 4) and control mice (n = 3) immediately before [^{123}I]IIMU injection (3.9-4.8 MBq). The hepatic accumulation levels of [^{123}I]IIMU was evaluated by SPECT/CT as described above.

2.9. Statistical analysis

All data are expressed as means ± standard deviation (SD). Statistical significance was determined using Welch's t-test or one-way analysis of variance (ANOVA) followed by Tukey-Kramer test. The level of significance was taken as $p < 0.05$. The tests were performed using GraphPad Prism software (GraphPad Software Inc., San Diego, CA).

3. Results

3.1. Physiological characteristics and hepatic pathology in NASH and control mice

Anthropometric and biochemical parameters in the MCD-diet-induced NASH and control mice are shown in Table 1. No significant difference in liver weight was observed between the NASH and control mice. The NASH mice showed a lower body weight ($p < 0.001$) and a higher liver/body weight ratio (%) ($p < 0.01$) than the control mice. Serum ALT and AST levels were significantly higher in the NASH mice than in the control mice ($p < 0.01$).

Figure 2 shows the hepatic expression levels of inflammation (TNF-α, IL-1β), Kupffer cell (CD68), and fibrosis (COL1A1, COL1A2, α-SMA) markers in the NASH and control mice. The expression levels of TNF-α, IL-1β, CD68, COL1A1, COL1A2, and α-SMA were significantly higher in the NASH mice than in the control mice. H&E-stained liver tissue sections from the NASH and control mice are shown in Fig. 3. Prominent steatosis, cellular infiltrations, and ballooning degeneration of hepatocytes were observed in the liver of the NASH mice but not in that of the control mice.

3.2. Hepatic TYMP and UPP expressions in NASH and control mice

The hepatic expression levels of TYMP were lower in the NASH mice than in the control mice at both mRNA [relative expression of mRNA: 1.00 ± 0.13 (Control) vs 0.43 ± 0.23 (NASH), $p < 0.01$] and protein levels [relative expression of protein: 1.00 ± 0.51 (Control) vs 0.14 ± 0.07 (NASH), $p < 0.05$] (Fig. 4). No UPP1 and UPP2 expressions were detected in the liver of the NASH and control mice, whereas recombinant UPP1 (1 ng) and UPP2 (10 ng) (positive controls) were clearly detected (Fig. S1).

3.3 Biodistribution analyses of [^{125}I]IIMU in NASH and control mice

The biodistributions of [^{125}I]IIMU in the NASH, control mice, 30 min after administration are shown in Fig. 5. [^{125}I]IIMU showed a markedly higher accumulation level in the liver than in other organs including the thymus, heart, lung, spleen, stomach, small intestine, large intestine, kidney, and thigh muscle (Fig. 5A). The hepatic accumulation level of [^{125}I]IIMU was significantly lower in the NASH mice than in the control mice [SUV: 6.65 ± 1.44 (Control) vs 3.36 ± 1.14 (NASH), $p < 0.05$; Fig. 5A].

The liver-to-blood ratios were also significantly lower in the NASH mice than in the control mice [58.3 ± 15.1 (Control) vs 33.8 ± 11.4 (NASH), $p < 0.05$; Fig. 5B]. The accumulation level and organ-to-blood ratios in the organs except for the liver were not significantly different between the NASH and control mice.

3.4. Hepatic localizations of [^{125}I]IIMU and TYMP protein in NASH and control mice

Representative hepatic ARG images of [^{125}I]IIMU and IHC staining images of TYMP are shown in Fig. 6. [^{125}I]IIMU was uniformly distributed in the liver of the control mice (Fig. 6A, panel a), whereas it showed a patchy distribution in the liver of the NASH mice (Fig. 6B, panel a). The hepatic localization of [^{125}I]IIMU was visually consistent with that of the TYMP protein in the control (Fig. 6A, panels a and b) and NASH mice (Fig. 6B, panels a and b).

3.5. SPECT/CT imaging of [^{123}I]IIMU in NASH and control mice

SPECT/CT images and mean hepatic [^{123}I]IIMU uptake values are shown in Fig. 7. The hepatic accumulation of [^{123}I]IIMU in the NASH mice was significantly lower than

296 that in the control mice [SUV (g/ml): 4.14 ± 0.87 (Control) vs 2.31 ± 0.29 (NASH), $p <$
297 0.01]. Blocking with TYMP inhibitor TIP significantly reduced the hepatic
298 accumulation of [^{123}I]IIMU in the both NASH and control mice [SUV (g/ml): 0.52 ±
299 0.42 (Control-TIP), 0.13 ± 0.05 (NASH-TIP), $p < 0.001$]. However, [^{123}I]IIMU SPECT
300 could not visualize a patchy distribution of TYMP in the liver of NASH.
301

4. Discussion

In this study, we investigated whether TYMP has a potential as an imaging biomarker and also evaluated the potential use of [^{123}I]IIMU for the diagnosis of NASH. This is the first study to evaluate the hepatic expression levels of TYMP in NASH mice and to examine the usability of a TYMP imaging probe for the evaluation of the state of NASH. We hypothesized that the expression levels of TYMP could be increased in the liver of NASH mice, because TYMP is induced by TNF-α, which plays a pivotal role in the development of fatty liver and subsequently NASH [5]. However, both the mRNA and protein expression levels of TYMP in the liver of NASH mice were decreased (Fig. 4). Moreover, as in the results of TYMP expression analyses, the hepatic accumulation levels of [^{125}I]IIMU were significantly lower in the NASH mice than in the control mice (Fig. 5). Furthermore, we found that [^{125}I]IIMU also showed a patchy distribution in the liver of NASH mice, and the distribution of [^{125}I]IIMU was visually consistent with that of the TYMP protein in the liver of NASH mice (Fig. 6). SPECT analysis also indicated that the hepatic accumulation levels of [^{123}I]IIMU were significantly lower in the NASH mice, and [^{123}I]IIMU SPECT can visually distinguish between the NASH and control mice (Fig. 7). Although these results were different from our initial hypothesis, they

suggested that SPECT imaging using [^{123}I]IIMU may be applicable to the noninvasive evaluation of the entire liver in NASH patients.

In this study, we utilized the MCD-diet-induced NASH as the disease model because it is one of the most widely used NASH models, in which the expression levels of TNF-α are also increased in the liver [17], and its hepatic histopathological changes are morphologically similar to those observed in NASH patients [18]. Also in our study, the main histopathological features of NASH, such as prominent steatosis, cellular infiltrations, and ballooning degeneration of hepatocytes, were observed in the liver of NASH mice, but not in that of control mice (Fig. 3). Moreover, the serum ALT and AST levels (Table 1) and the hepatic expression levels of markers of inflammation (including TNF-α), Kupffer cells, and fibrosis (Fig. 2) were significantly higher in the NASH mice than in the control mice, indicating that the NASH model was successfully prepared in our study.

In our previous studies, we clearly demonstrated that TYMP mRNA and protein were more highly expressed in the normal liver and small intestine than in the other organs including the heart, lung, stomach, spleen, kidney, large intestine, muscle, and brain [12]. Radiolabeled IIMU also accumulated mostly in the liver and small intestine of mice [9, 10, 12]. Moreover, the hepatic accumulation level of this probe was reduced to

15% in blocking experiments with non-radiolabeled IIMU [10]. These results in these studies indicate that the high accumulation levels of radiolabeled IIMU in the liver and small intestine are attributable to its binding to the TYMP physiologically expressed in the organs. Also in this study, radiolabeled IIMU accumulated mostly in the liver and small intestine compared with the other organs, which is consistent with the results of our previous studies. The ARG and IHC studies also indicated that the hepatic distribution of [^{125}I]IIMU in the NASH and control mice was visually consistent with that of the TYMP protein (Fig. 6).

Since liver is a main organ involved in drug metabolism, [$^{123/125}$I]IIMU has the potential to be metabolized in the liver and accumulate in it nonspecifically. However, the metabolite analysis of it in the liver has not been conducted. This is a limitation of our study. On the other hand, we performed the blocking study in NASH and control mice using TIP (TYMP inhibitor), to confirm whether [^{123}I]IIMU accumulates in the liver specifically (Fig. 7). TIP is also a uracil derivative and has a similar structure of IIMU. Therefore, it is expected that the hepatic accumulation of IIMU is inhibited by TIP when the accumulation is specific to TYMP. This blocking study also indicated that the hepatic accumulation of [^{123}I]IIMU in the both NASH and control mice is significantly reduced (Fig. 7B). This result suggested that most hepatic accumulation of

356 [^{123}I]IIMU in the both NASH and control mice is specific and not due to hepatic
357 metabolism (non-specific).

358 Furthermore, since mouse UPPs also have TYMP activity unlike human UPPs [19],
359 [$^{123/125}$I]IIMU has potential to accumulate organs expressing the UPPs. Although the
360 activity is not necessarily proportional to the expression level, an organ with the highest
361 TYMP activity derived from UPPs is a small intestine [19] and hence the observed
362 accumulation of IIMU in the small intestine may be partly due to UPPs. On the other
363 hand, our study clearly indicated that no UPP1 and UPP2 expressions were detected in
364 the liver of the NASH and control mice (Fig. S1), indicating that UPPs are not involved
365 in the accumulation of the TYMP imaging probe in the liver. These results supported
366 the finding that [$^{123/125}$I]IIMU binds specifically to TYMP in the liver of the NASH and
367 control mice.

368 A key question not addressed in this study is the reason why the hepatic expression
369 levels of TYMP were lower in the NASH mice than in the control mice, even when the
370 TNF-α expression levels were higher in the NASH mice. Although the reason for this
371 unexpected finding is currently unknown, it strongly suggests that certain TYMP
372 downregulators, which are more potent than TNF-α, may exist in the liver of NASH
373 mice. In the NASH liver, the repetitive cycles of hepatic injury and enhanced

374 compensatory regeneration/proliferation of hepatocytes occur, which may lead to the
375 increased demand for thymidine. Since TYMP is a key enzyme involved in the
376 thymidine salvage pathway [20] and a recent study suggested that TYMP lowers the
377 thymidine levels within the hepatocytes [21], it is possible to consider that the increase
378 in thymidine requirement suppressed the hepatic expression levels of TYMP in NASH
379 mice. Further mechanistic studies are warranted to evaluate this possibility.

380 Although the MCD-diet-induced NASH is commonly used as the disease model in
381 basic research, the problems with these mice are their body weight loss and lack of
382 insulin resistance [22], which are well-known symptoms in patients with NASH. It is
383 necessary to examine in future experiments whether obesity and insulin resistance affect
384 the thymidine metabolism and biodistribution of [^{123}]IIMU.

385 Other imaging techniques such as MRI and CT can assess the hepatic steatosis with
386 higher spatial resolution image in comparison with SPECT. Therefore, further studies
387 are needed to find advantages of [^{123}I]IIMU for imaging NASH. As a potential
388 advantage, unlike the liver with NASH, several cancers including HCC highly express
389 TYMP, in comparison with normal organs [20, 23]. Therefore, [^{123}I]IIMU may be used
390 for the clear discrimination between NASH and NASH-related HCC. Further studies
391 are currently under way to examine how the expression levels of TYMP change

according to the progression of NASH.

5. Conclusions

In this study, we demonstrated that the hepatic accumulation levels of [^{125}I]IIMU were decreased with a patchy distribution in NASH mice. These results were consistent with the expression level and localization of TYMP in the liver. These results also suggest the feasibility of TYMP as an imaging biomarker of NASH. Moreover, SPECT imaging using [^{123}I]IIMU may provide a noninvasive means for the diagnosis of NASH.

Acknowledgments

The authors thank Ms. Yukiko Komatsu and Ms. Yoko Ebita for their technical support in the synthesis of [^{125}I]IIMU. This study was supported in part by Grants-in-Aid for Scientific Research (Grant number: 15H06001 and 19K17255) from the Japan Society for the Promotion of Science and the Ministry of Education, Culture, Sports, Science, and Technology, Japan.

Conflict of Interest Statement

Kazue Ohkura, Yuji Kuge, Hokkaido University, Health Sciences University of Hokkaido, and Nihon Medi-Physics Co.,Ltd. have patent rights for [^{123}I]IIMU. Yuji Kuge has received grants from Nihon Medi-Physics Co.,Ltd., outside the submitted work. There are no other potential conflicts of interest relevant to this article.

References

1. Bedossa P. Diagnosis of non-alcoholic fatty liver disease/non-alcoholic steatohepatitis: Why liver biopsy is essential. Liver Int 2018;38 Suppl 1:64-6.
2. Sumida Y, Nakajima A, and Itoh Y. Limitations of liver biopsy and non-invasive diagnostic tests for the diagnosis of nonalcoholic fatty liver disease/nonalcoholic steatohepatitis. World J Gastroenterol 2014;20:475-85.
3. Gawrieh S, Knoedler DM, Saeian K, Wallace JR, and Komorowski RA. Effects of interventions on intra- and interobserver agreement on interpretation of nonalcoholic fatty liver disease histology. Ann Diagn Pathol 2011;15:19-24.
4. Younossi ZM, Gramlich T, Liu YC, Matteoni C, Petrelli M, Goldblum J, et al. Nonalcoholic fatty liver disease: assessment of variability in pathologic interpretations. Mod Pathol 1998;11:560-5.
5. Tsochatzis EA, Papatheodoridis GV, and Archimandritis AJ. Adipokines in nonalcoholic steatohepatitis: from pathogenesis to implications in diagnosis and therapy. Mediators Inflamm 2009;2009:831670.
6. Li Z, Yang S, Lin H, Huang J, Watkins PA, Moser AB, et al. Probiotics and antibodies to TNF inhibit inflammatory activity and improve nonalcoholic fatty

liver disease. Hepatology 2003;37:343-50.

7. Toi M, Rahman MA, Bando H, and Chow LWC. Thymidine phosphorylase (platelet-derived endothelial-cell growth factor) in cancer biology and treatment. The Lancet Oncol 2005;6:158-66.

8. Toyoda Y, Tabata S, Kishi J, Kuramoto T, Mitsuhashi A, Saijo A, et al. Thymidine phosphorylase regulates the expression of CXCL10 in rheumatoid arthritis fibroblast-like synoviocytes. Arthritis Rheumatol 2014;66:560-8.

9. Takahashi M, Seki K-i, Nishijima K-i, Zhao S, Kuge Y, Tamaki N, et al. Synthesis of a radioiodinated thymidine phosphorylase inhibitor and its preliminary evaluation as a potential SPECT tracer for angiogenic enzyme expression. J Labelled Comp Radiopharm 2008;51:384-7.

10. Akizawa H, Zhao S, Takahashi M, Nishijima K, Kuge Y, Tamaki N, et al. In vitro and in vivo evaluations of a radioiodinated thymidine phosphorylase inhibitor as a tumor diagnostic agent for angiogenic enzyme imaging. Nucl Med Biol 2010;37:427-32.

11. Li H, Zhao SJ, Jin YN, Nishijima K, Akizawa H, Ohkura K, et al. Radiolabeled uracil derivative as a novel SPECT probe for thymidine phosphorylase: suppressed accumulation into tumor cells by target gene knockdown. Nucl Med Commun

2011;32:1211-5.

12. Zhao S, Li H, Nishijima K, Zhao Y, Akizawa H, Shimizu Y, et al. Relationship between biodistribution of a novel thymidine phosphorylase (TP) imaging probe and TP expression levels in normal mice. Ann Nucl Med 2015;29:582-7.
13. Kobashi N, Matsumoto H, Zhao S, Meike S, Okumura Y, Abe T, et al. The Thymidine Phosphorylase Imaging Agent ^{123}I-IIMU Predicts the Efficacy of Capecitabine. J Nucl Med 2016;57:1276-81.
14. Watanabe S, Hirata K, Shiga T, Toyonaga T, Okamoto S, Uchiyama Y et al. First-in-Human Study of a Novel Thymidine Phosphorylase Tracer [^{123}I]IIMU in Healthy Volunteers - Preliminary Report. J Nucl Med 2016;57:449.
15. Higashikawa K, Akada N, Yagi K, Watanabe K, Kamino S, Kanayama Y, et al. Exploration of target molecules for molecular imaging of inflammatory bowel disease. Biochem Biophys Res Commun 2011;410:416-21.
16. Higashikawa K, Yagi K, Watanabe K, Kamino S, Ueda M, Hiromura M, et al. 64Cu-DOTA-anti-CTLA-4 mAb enabled PET visualization of CTLA-4 on the T-cell infiltrating tumor tissues. PLoS One 2014;9:e109866.
17. Rolla S, Alchera E, Imarisio C, Bardina V, Valente G, Cappello P, et al. The balance between IL-17 and IL-22 produced by liver-infiltrating T-helper cells critically

controls NASH development in mice. Clin Sci (Lond) 2016;130:193-203.

18. Li H, Toth E, and Cherrington NJ. Asking the Right Questions With Animal Models: Methionine- and Choline-Deficient Model in Predicting Adverse Drug Reactions in Human NASH. Toxicol Sci 2018;161:23-33.

19. Haraguchi M, Tsujimoto H, Fukushima M, Higuchi I, Kuribayashi H, Utsumi H, et al. Targeted Deletion of Both Thymidine Phosphorylase and Uridine Phosphorylase and Consequent Disorders in Mice. Mol Cell Biol 2002;22:5212-21.

20. Elamin YY, Rafee S, Osman N, KJ OB, and Gately K. Thymidine Phosphorylase in Cancer; Enemy or Friend? Cancer Microenviron 2016;9:33-43.

21. Tabata S, Yamamoto M, Goto H, Hirayama A, Ohishi M, Kuramoto T, et al. Thymidine Catabolism as a Metabolic Strategy for Cancer Survival. Cell Rep 2017;19:1313-21.

22. Rinella ME and Green RM. The methionine-choline deficient dietary model of steatohepatitis does not exhibit insulin resistance. J Hepatol 2004;40:47-51.

23. Morinaga S, Yamamoto Y, Noguchi Y, Imada T, Rino Y, Akaike M, et al. Platelet-derived endothelial cell growth factor (PD-ECGF) is up-regulated in human hepatocellular carcinoma (HCC) and the corresponding hepatitis liver. Hepato-Gastroenterol 2003;50:1521-6.

Figure legends

Figure 1: Chemical structure of radioiodine-labeled 5-iodo-6-[(2-iminoimidazolidinyl)methyl] uracil (IIMU). The *I in the structure indicates the position of radioiodine.

Figure 2: Gene expression analysis in liver tissues from NASH and control mice by real-time RT-PCR. Relative hepatic expression levels of inflammatory (TNF-α, IL-1β), Kupffer cell (CD68), and fibrosis (COL1A1, COL1A2, α-SMA) markers in NASH (n = 5) and control (n = 5) mice. Each expression level was normalized to that of TBP, and each bar represents means ± SD. For statistical evaluation, Welch's t-test was applied. The symbols ** and *** denote $p < 0.01$ and $p < 0.001$ vs control mice, respectively.

Figure 3: Assessment of histopathological findings of livers from NASH and control mice. A. Microscopic observations of the liver from control mice (n = 3). B. Microscopic observations of the liver from NASH mice (n = 3). Representative H&E-stained liver sections are shown. Scale bar = 100 μm. The yellow and blue arrows indicate cellular infiltration and ballooning degeneration of hepatocytes, respectively.

Figure 4: TYMP expression in liver tissues from NASH and control mice evaluated by real-time RT-PCR and western blot analyses. A. mRNA expression levels of TYMP in the livers from NASH (n = 5) and control (n = 5) mice. Each TYMP expression level was normalized to that of TBP, and each bar represents mean ± SD. For statistical evaluation, Welch's t-test was applied. The symbol ** denotes $p < 0.01$ vs control mice. B. Representative western blot images of TYMP in the livers from NASH (n = 5) and control (n = 5) mice (left), and the densitometric quantification values of the immunoblot bands (right). The expression level of TBP is shown as an internal control.

Figure 5: Biodistribution analyses of [^{125}I]IIMU in NASH and control mice. A. SUVs of [^{125}I]IIMU in NASH (n = 4) and control (n = 4) mice. B. Organ-to-blood ratios of [^{125}I]IIMU in NASH (n = 4) and control (n = 4) mice. For statistical evaluation, Welch's t-test was applied. Data are expressed as means ± SD. The symbol * denotes $p < 0.05$ vs control mice.

Figure 6: Hepatic localizations of TYMP and [^{125}I]IIMU in NASH and control mice. A. Representative ARG images of [^{125}I]IIMU in the liver of a control mouse (panel a; n = 4). Representative IHC staining images of TYMP in the liver from a control mouse (panel b; n = 4). B. Representative ARG images of [^{125}I]IIMU in the liver from a NASH

mouse (panel a; n = 4). Representative IHC staining images of TYMP in the liver of a NASH mouse (panel b; n = 4). The yellow arrows indicate similar hepatic distribution patterns of [^{125}I]IIMU and TYMP protein in a NASH mouse. Scale bar (blue) = 2.0 mm.

Figure 7: SPECT/CT analyses of [^{123}I]IIMU in NASH and control mice. A. Representative SPECT/CT images of [^{123}I]IIMU in the NASH and control mice with or without blockade of TIP (TYMP inhibitor) at 30 min post injection under isoflurane anaesthesia (3.3-4.8 MBq injected dose). The imaging time was 15 min. B. Hepatic accumulation levels of [^{123}I]IIMU in NASH and control mice with or without blockade of TIP. Data are expressed as means ± SD (n = 3-4, for each). For statistical evaluation, one-way ANOVA followed by Tukey-Kramer test was applied. The symbols ** and *** denote $p < 0.01$ and $p < 0.001$ vs control mice, respectively.

Table 1: Biochemical parameters of MCD-diet-induced NASH and control mice.

	Control	NASH
Serum ALT (U/L)	30.6 ± 8.3	254.9 ± 76.4**
Serum AST (U/L)	58.9 ± 13.2	89.4 ± 12.7**

ALT, alanine aminotransferase; AST, aspartate transaminase.

Data are expressed as means ± standard deviation (SD). For statistical evaluation, Welch's t-test was applied. The symbols ** denotes $p < 0.01$ vs control mice, respectively. n = 5.

Figure 1

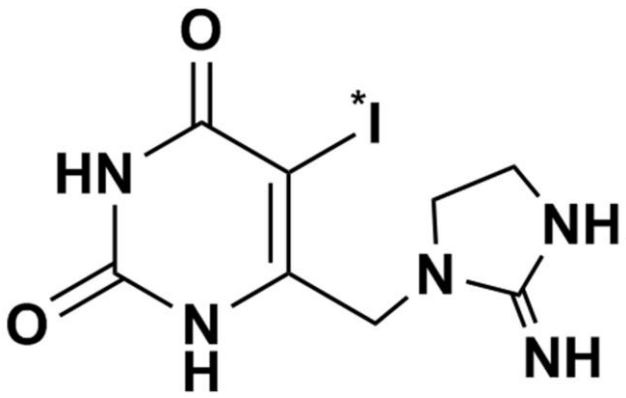

Figure 2

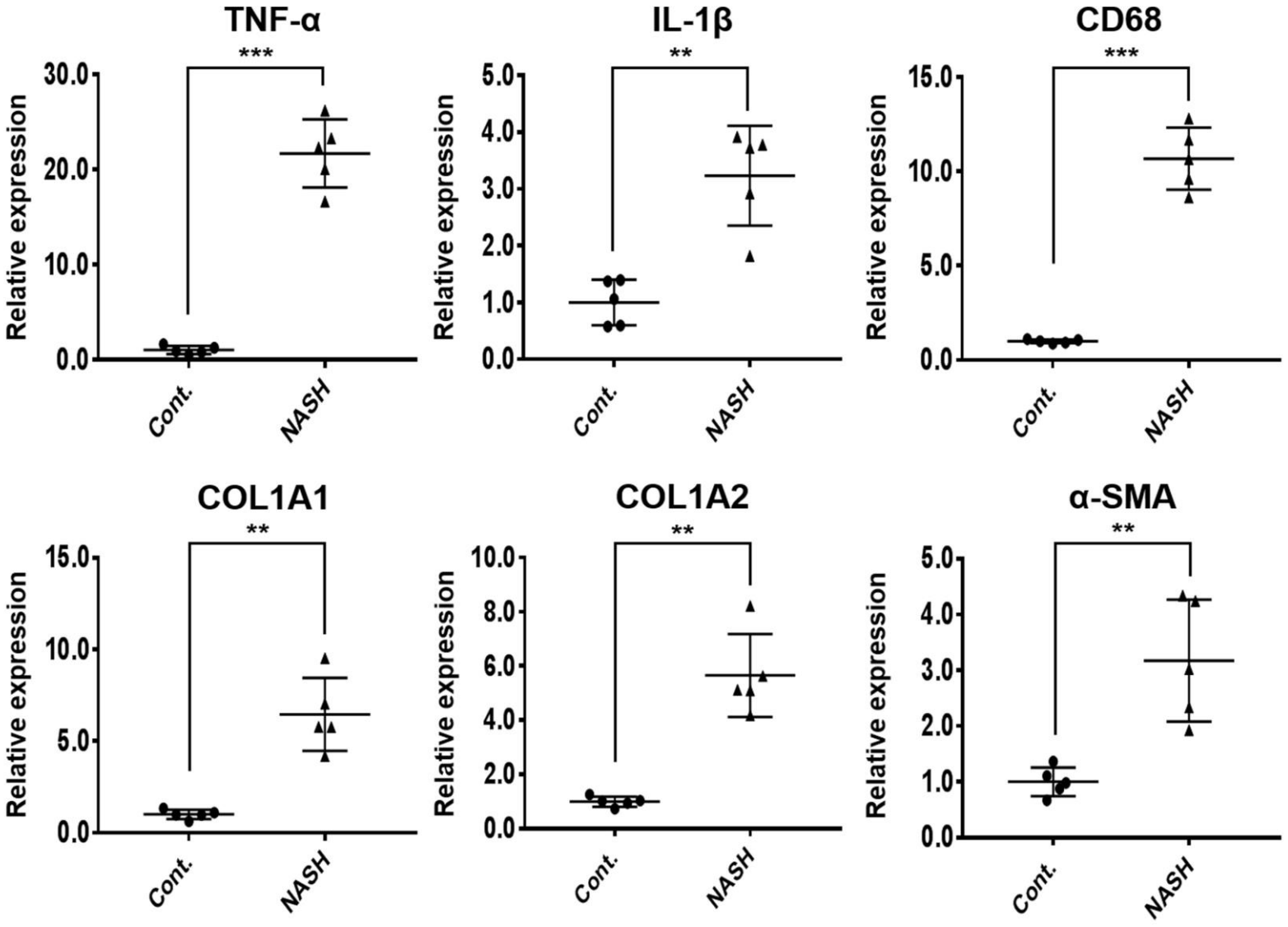
TNF-α
***
Relative expression
30.0
20.0
10.0
0.0
Cont.
NASH
IL-1β
**
Relative expression
5.0
4.0
3.0
2.0
1.0
0.0
Cont.
NASH
CD68
***
Relative expression
15.0
10.0
5.0
0.0
Cont.
NASH
COL1A1
**
Relative expression
15.0
10.0
5.0
0.0
Cont.
NASH
COL1A2
**
Relative expression
10.0
8.0
6.0
4.0
2.0
0.0
Cont.
NASH
α-SMA
**
Relative expression
5.0
4.0
3.0
2.0
1.0
0.0
Cont.
NASH

Figure 3

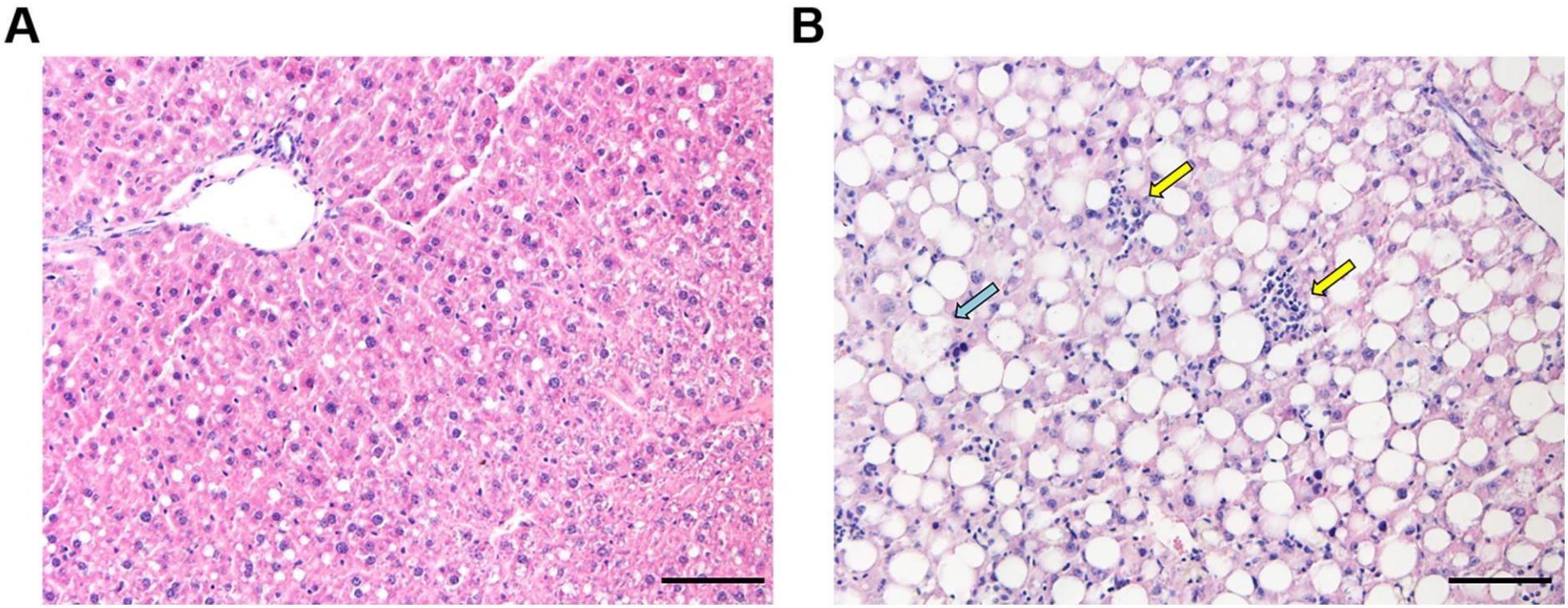

Figure 4

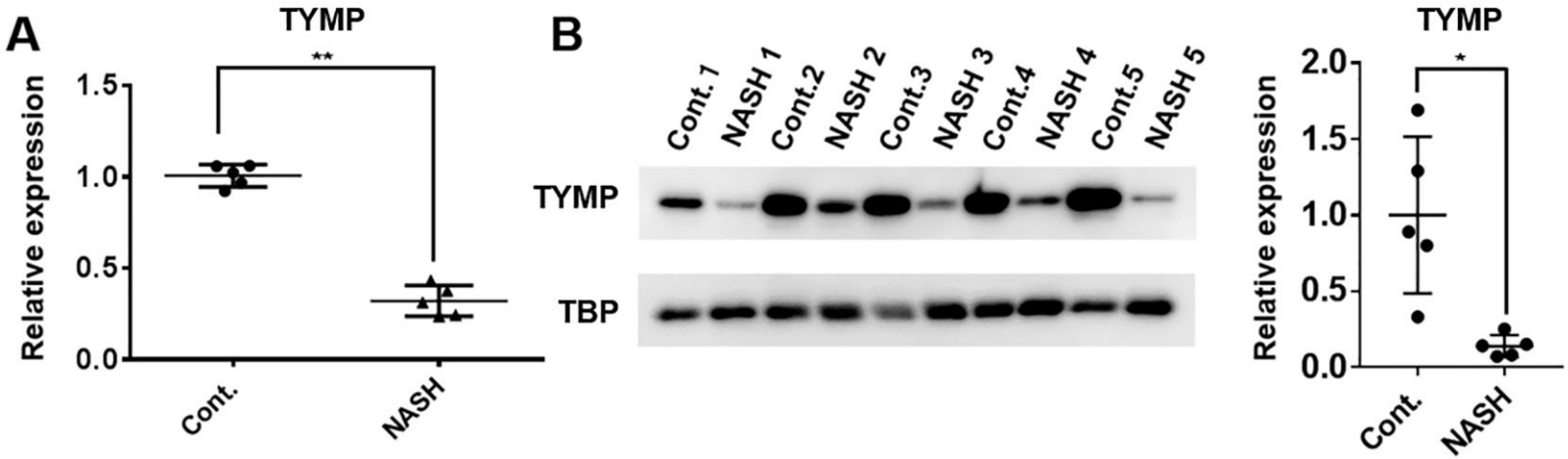
A
TYMP
**
Relative expression
1.5
1.0
0.5
0.0
Cont.
NASH
B
Cont. 1
NASH 1
Cont.2
NASH 2
Cont.3
NASH 3
Cont.4
NASH 4
Cont.5
NASH 5
TYMP
TBP
TYMP
*
Relative expression
2.0
1.5
1.0
0.5
0.0
Cont.
NASH

Figure 5

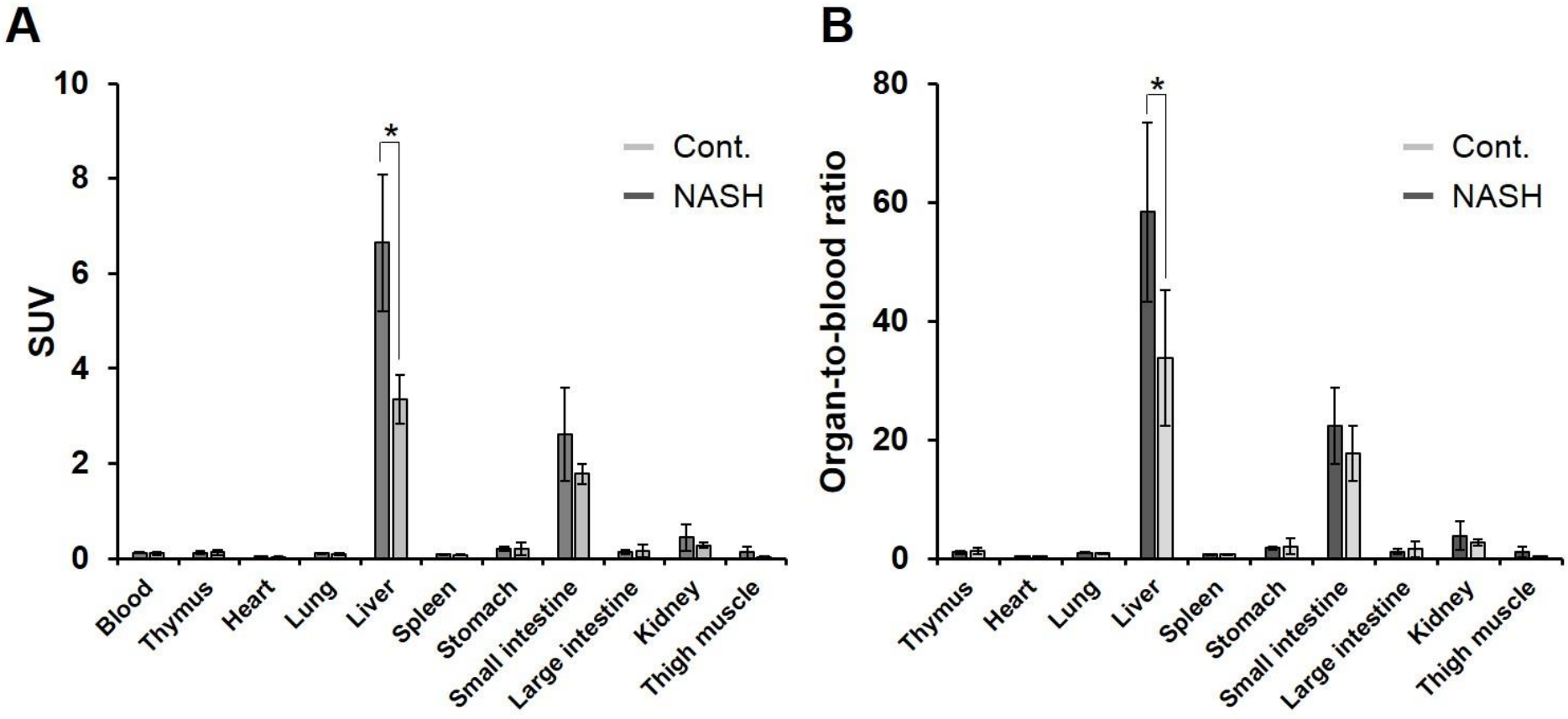
A
SUV
10
8
6
4
2
0
*
Cont.
NASH
Blood
Thymus
Heart
Lung
Liver
Spleen
Stomach
Small intestine
Large intestine
Kidney
Thigh muscle
B
Organ-to-blood ratio
80
60
40
20
0
*
Cont.
NASH
Thymus
Heart
Lung
Liver
Spleen
Stomach
Small intestine
Large intestine
Kidney
Thigh muscle

Figure 6

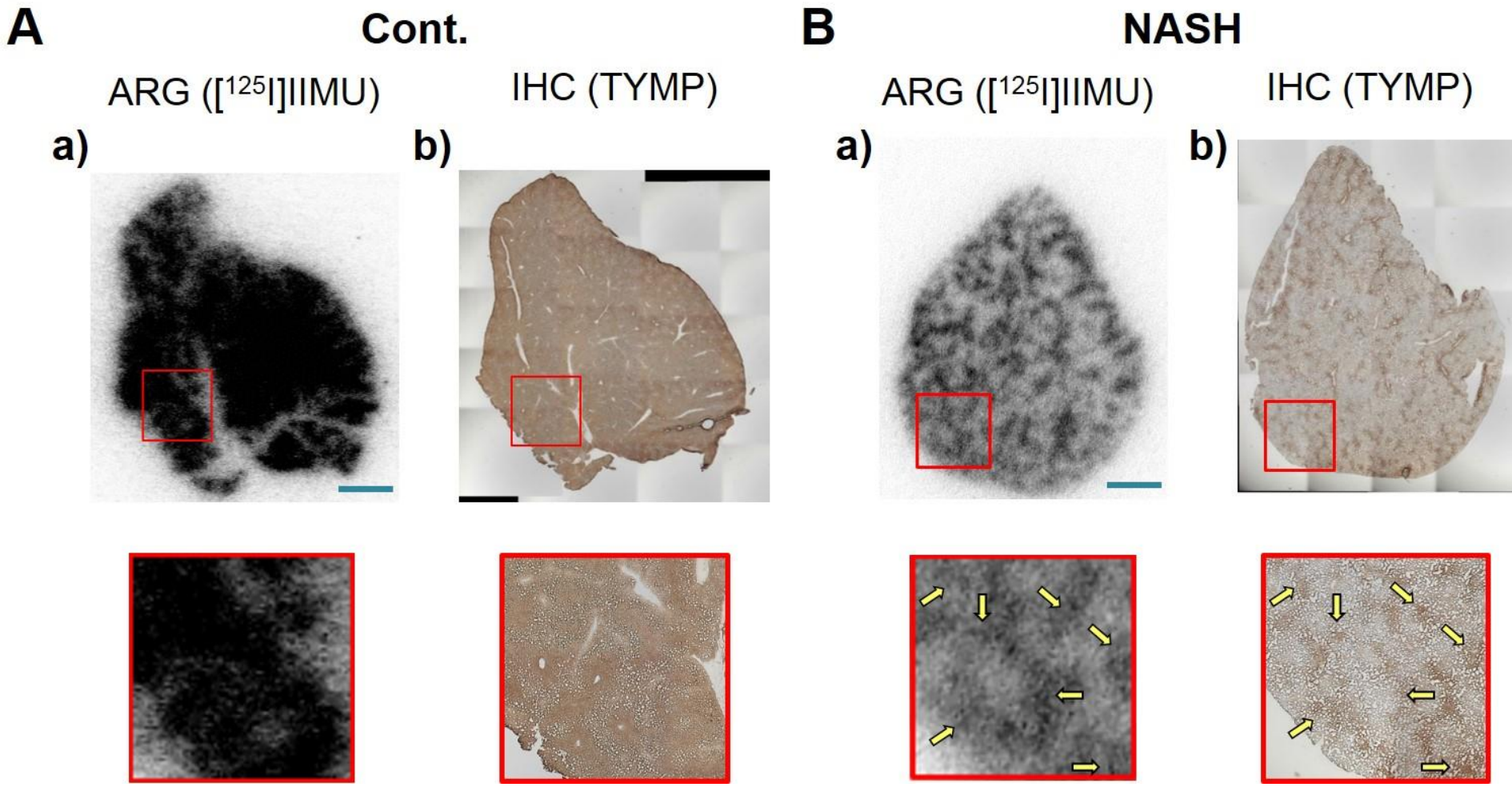
A
Cont.
ARG ([125I]IIMU)
IHC (TYMP)
a)
b)
B
NASH
ARG ([125I]IIMU)
IHC (TYMP)
a)
b)

Figure 7

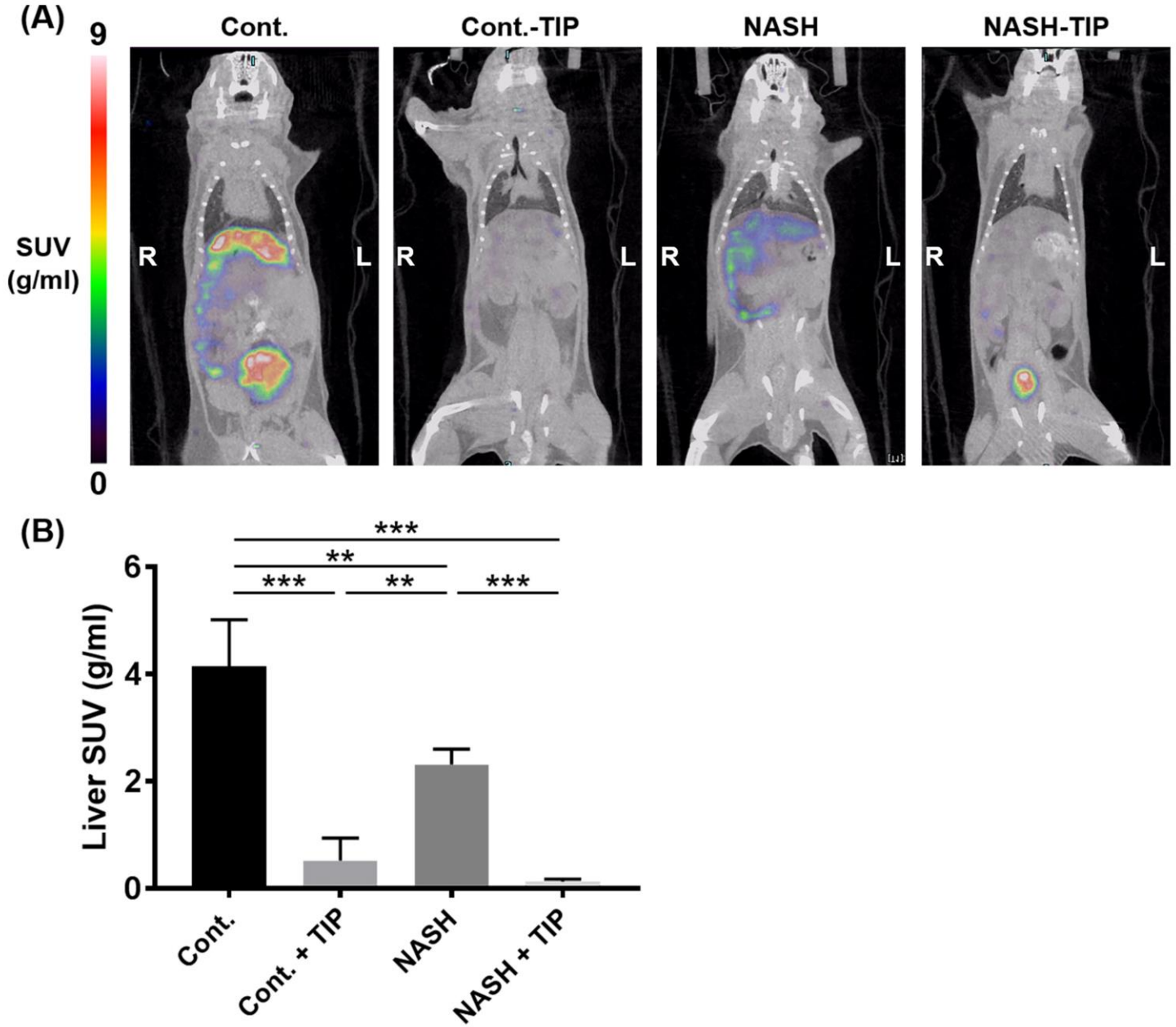
(A)
9
SUV
(g/ml)
0
Cont.
Cont.-TIP
NASH
NASH-TIP
R
L
(B)
***
**
***
**
***
Liver SUV (g/ml)
6
4
2
0
Cont.
Cont. + TIP
NASH
NASH + TIP